Testing and Modeling of a New Moment Connection of Concrete-Filled FRP Tubes to Footings under Monotonic and Cyclic...

Article *in* Journal of Composites for Construction · August 2011

DOI: 10.1061/(ASCE)CC.1943-5614.0000198

CITATIONS
2

READS
5

3 authors, including:

Pedram Sadeghian
Dalhousie University
28 PUBLICATIONS **78** CITATIONS
SEE PROFILE

Amir Fam
Queen's University
189 PUBLICATIONS **2,037** CITATIONS
SEE PROFILE

Testing and Modeling of a New Moment Connection of Concrete-Filled FRP Tubes to Footings under Monotonic and Cyclic Loadings

Pedram Sadeghian, M.ASCE[1]; Yu Ching Lai[2]; and Amir Fam, M.ASCE[3]

ABSTRACT

This study explores a new moment connection of concrete-filled FRP tube (CFFT) to concrete footing. The tube is tightly fitted and adhesively bonded to a short reinforced concrete stub protruding from footing, which facilitates concrete filling of the tube without the need for shoring. To establish the critical stub length (X_{cr}), specimens with heavily steel-reinforced stubs varying in length from 0.5D to 2.0D, where D is the diameter, were fabricated and tested in flexure using a cantilever setup. The X_{cr} required to achieve flexural failure of the CFFT was 1.05D. Additional specimens with a sufficient stub length of 1.5D were then fabricated to examine the effect of steel reinforcement ratio (ρ_s) in the stub, on strength and ductility. The optimal ρ_s of stub required for the CFFT to reach flexural failure was 3.2%. Finally, the effect of low-cycle reversed bending fatigue was studied with and without axial compression load. Remarkable ductility associated with the formation of a plastic hinge was observed at ρ_s of 2%. An analytical model capable of predicting moment capacity of the connection, whether failure is governed by flexure or bond, and also predict X_{cr}, was developed and validated. It was then used in a parametric study to explore the effects of CFFT mechanical and geometric properties on X_{cr}.

Keywords: Concrete-filled, tube, CFFT, connection, footing, bond, ductility, cyclic.

---

[1] Postdoctoral Fellow, Department of Civil Engineering, Queen's University, Kingston, ON, K7L 3N6 Canada. E-mail: p.sadeghian@queensu.ca
[2] Former Master's Student, Department of Civil Engineering, Queen's University, Kingston, ON, K7L 3N6 Canada. E-mail: yuching.lai@ce.queensu.ca
[3] Professor and Canada Research Chair in Innovative and Retrofitted Structures, Department of Civil Engineering, Queen's University, Kingston, ON, K7L 3N6 Canada. E-mail: fam@civil.queensu.ca

INTRODUCTION

Fiber reinforced polymers (FRPs) can be produced in a variety of forms. One of which is hollow tubes, which can be used as stay-in-place structural forms in the concrete filled FRP tube (CFFT) system. The system eliminates the need for conventional concrete forms, lending itself to accelerated construction and the tube can fully or partially replaces conventional reinforcement, eliminating or reducing the risk of steel corrosion (Mirmiran and Shahawy, 1997; and Fam and Rizkalla, 2002). The system is suitable for both cast-in-place and precast industries (Zhu et al., 2004 and 2006; Qasrawi and Fam, 2008; and Fam, 2008). Current and potential applications of CFFTs are as piles, bridge piers, and utility poles. A key factor in the success of the system is the development of proper moment connections of the CFFT member to other components.

Zhu et al. (2004) studied three types of CFFT connections in precast modular bridge frames, namely male-female, dowel bars with or without embedment, and post-tensioning connections. The feasibility of the precast modular system and connections was demonstrated in that study. Zhu et al. (2006) studied seismic performance of different CFFT column-footing connections, namely a cast-in-place CFFT column with starter bars extending from the footing, a precast CFFT column with starter bars from the footing inserted into grouted ducts, and a precast CFFT column post-tensioned to the footing with unbonded high strength rods. All CFFTs were embedded into the footings at the same depth. The CFFT columns exhibited significant improvement in strength and ductility over conventional RC columns. Nelson et al. (2008) tested CFFT cantilevered specimens embedded into footings at various depths, without any dowel-bars. It was shown that the minimum embedment required to achieve flexural failure was 0.73 the diameter but it also depends on the tube properties. A robust model was later developed for this

connection by Sadeghian and Fam (2010) and was able to establish the critical embedment length required for any combination of moment, axial load, and shear load.

This study presents an experimental investigation into a new CFFT moment connection to RC footings. The hollow FRP tube is 'fitted over' and adhesively bonded to a short RC stub protruding from the footing. The diameter of the RC stub is slightly smaller than the inner diameter of the FRP tube. The outer surface of the stub and the inner surface of the tube end are coated with a viscous adhesive, before the tube is fitted over the stub. In current practice, any CFFT system still requires shoring of the tube during concrete filling. In the proposed method, the tube is stable without the need for any shoring during curing of the adhesive or subsequent concrete filling, because of the tight fit over the stub. As such, the proposed connection aims to further simply constructability and take full advantage of the stay-in-place form.

EXPERIMENTAL PROGRAM

The experimental program was designed to achieve three goals: (a) establish the minimum length of the RC stub required to develop the full moment capacity of the CFFT member, such that bond failure at the tube-stub interface is avoided (Phase I), (b) study the effect of the conventional steel reinforcement ratio in the stub, on the strength and ductility of the system (Phase II), and (c) study the connection under reversed cyclic loading with and without axial loading (Phase III). CFFT-footing cantilever specimens were fabricated and tested under lateral loading applied at the free end of the CFFT (Fig. 1). Each specimen had a 500×500×500 mm RC footing with a protruding 159 mm diameter RC stub, and a 169 mm outer diameter CFFT member with a 1300 mm span between the loading point and the footing. The stub diameter was slightly smaller than the 162 mm inner diameter of the FRP tube. The RC stubs varied in length and internal steel reinforcement ratio. No steel reinforcement was provided in the CFFT.

Test Specimens and Parameters

Table 1 provides summary of the test matrix. In phase I, four specimens (M-0.5D-S9, M-1.0D-S9, M-1.5D-S9, and M-2.0D-S9) with varying RC stub lengths of 0.5 to 2.0 times the diameter of the CFFT (i.e. 0.5*D* to 2.0*D*) were tested. Each RC stub was heavily reinforced with 6-20M steel bars (8.73% reinforcement ratio) connecting the stub to the footing, to insure that failure occurs either by flexure in the CFFT member just outside the stub or by bond between the FRP tube and stub. In Phase II, two additional specimens (M-1.5D-S4 and M-1.5D-S2) were fabricated with two different and rather more practical steel reinforcement ratios in the stubs, 3.88% (4-15M bars) and 1.94% (4-10M bars), respectively. The stub length was 1.5*D* in both specimens, slightly longer than the optimum length obtained in Phase I to avoid bond failure. In Phase III, two specimens (C-1.5D-S2 and PC-1.5D-S2), identical to M-1.5D-S2, were tested under reversed cyclic loading, with PC-1.5D-S2 externally post-tensioned to provide an axial compression load of 15% of the CFFT ultimate axial strength during cyclic loading. In order to establish the CFFT axial strength, a 700 mm long CFFT stub was fabricated and tested to failure under axial compression load.

Material Properties

GFRP Tube: The GFRP tube used in all specimens had a 169 mm outer diameter, a 3.5 mm wall thickness and comprised nine E-glass-epoxy layers in alternating angles of 9° and 86° with respect to the longitudinal axis. Tension tests were performed on the GFRP tubes using three longitudinal coupons of 25 mm width, 25 mm gauge length and 115 mm tabs at both ends for gripping. Strains were measured on both sides of the coupons. The coupons showed slightly non-linear stress-strain behavior (Fig. 2) with an average initial modulus of 17.8 GPa. Because of the fibers angles, the coupons failed slightly prematurely as indicated by the failure strain of 0.013,

which is lower than the average measured strain at tension failure in the CFFT members (0.02). As such, the ultimate tensile strength of the tube is estimated as 260 MPa.

Concrete: Ready-mix concrete with high-early strength cement, 14 mm maximum aggregate size, and a 150 mm slump, was used. The same mixture, with 35 MPa design strength, was used for the footings and the CFFT member. The average compressive strength at time of testing was 38 MPa for specimens in Phase I and 32 MPa for specimens in Phases II and III.

Epoxy Adhesive: Epoxy adhesive was used to bond the hollow GFRP tubes to the RC stubs. The adhesive is characterized by a viscous, mortar-like texture, which made it suitable to apply to the vertical surface of the RC stub and the inner surface of the tube. The reported bond tensile and shear strengths were 4 MPa and 15 MPa, respectively.

Steel Reinforcement: Standard 10M, 15M, and 25M steel rebar with cross-section areas of 100 mm^2, 200 mm^2, and 300 mm^2, respectively, were used to reinforce the footings and RC stubs. The average yield and ultimate strengths were 425 MPa and 680 MPa, respectively. Steel spirals in the RC stubs had a 150 mm outer diameter, a 50 mm pitch, and were fabricated from 5 mm diameter smooth steel wire. External prestressing of specimen PC-1.5D-S2 was applied using 15.2 mm diameter seven-wire steel strands of 1720 MPa nominal ultimate strength.

Fabrication of Test Specimens

Figure 3 shows the fabrication process of the RC footings with stubs. The 500×500×500 mm footings were heavily reinforced in the two directions, to avoid local failure in the footing. The dowel reinforcement of the stub was embedded into the footings. For specimen PC-1.5D-S2, two 25 mm diameter ducts were embedded in the footing to facilitate applying the axial force by post-tensioning. Short SonoTubes with a 159 mm inner diameter were secured in place to form the stubs. The footing and the stub were then cast virtually at the same time. The diameter of the

stub was designed to ensure proper fitting of the hollow GFRP tube over the stub, and allow for a 1.5 mm thick gap to accommodate a thin layer of the epoxy adhesive. The GFRP tubes were cut to a length of 1400 mm each and were installed after concrete curing and removal of the SonoTubes from the stubs. A layer of the epoxy adhesive was applied to the outer surface of the RC stub. Another layer was applied to the inner surface of the GFRP tube end. The GFRP tube was then slowly fitted over the RC stub in a spiral downward motion to ensure proper spread of the adhesive over the contact surface area. The tube was quite stable without the need for any additional shoring. After curing of the adhesive, the tube was filled with plain concrete.

External post-tensioning of specimen PC-1.5D-S2 was achieved using the setup shown in Fig. 4. The two steel strands were passed through the ducts in the footing and anchored at the back side of the footing with load cells installed between the anchors and bearing plates. At the CFFT free end, a rigid HSS steel beam was used to jack and then anchor the strands against. A hydraulic jack was used to apply the load. Special devices comprising short threaded rods and nuts were incorporated with the anchors to independently adjust the forces in each strand, to ensure equal forces. The force change overtime and during the test was monitored using the load cells installed at the dead end of each strand.

Test Setup and Instrumentation

All specimens were tested in a horizontal cantilever setting with a 1300 mm long moment arm (Fig. 5). A 1000 kN testing machine was used to apply load transversely at the free end, at a rate of 1.5 mm/min for the monotonically loaded specimens and up to 30 mm/min for cyclically loaded specimens. The RC footing was clamped to the test machine using a set of stiff steel sections and threaded rods. At the loading end, a steel ring with a welded grooved plate was fitted to the CFFT to accommodate a rounded knife-edge loading plate attached to the moving

cross-head of the machine. For cyclically loaded specimens, the end of the CFFT was clamped to a special swivel joint head to provide the push-pull action with free rotation.

Electrical resistance foil strain gauges and 100 mm displacement type strain gauge transducers were used to measure longitudinal strains on the tension and compression sides of the GFRP tube along its length, including the end of stub critical location. Deflection was measured using linear potentiometers (LPs) at the free end. Two additional LPs were used to measure the horizontal displacements between the end of the GFRP tube and footing, which comprise any slip between the GFRP tube and stub and also the flexural crack opening at the stub-footing junction. This measurement will be referred to as 'slip' in the plots. For specimen PC-1.5D-S2, strain gauges were installed on the prestressing strands, and load cells were installed at the dead end as indicated earlier, to record axial loads during jacking and testing. Further details of the experimental program are available in Lai (2010).

EXPERIMENTAL RESULTS AND DISCUSSION

The following sections present the flexural behavior and failure modes of the system with emphasis on the effects of stub length, stub reinforcement ratio and reversed cyclic loading. A summary of test results is given in Table 2.

The Effect of RC Stub Length (Phase I)

The specimens in Phase I had RC stubs varying in length from 0.5 to 2.0 times the CFFT diameter. Figure 6 shows a comparison of load-deflection responses at the free end, load-slip of the tube at the footing face, and load-longitudinal strains of the tube at the end of the RC stub. ***Bond Failure versus Flexural Failure:*** Failure modes of the specimens in this phase are shown in Fig. 7(a and b). Two distinctly different failure modes were observed. The two specimens with

shorter RC stub lengths of 0.5*D* and 1.0*D* experienced a bond failure of the tube over the RC stub length (Fig. 7(a)). This premature failure occurred before the CFFT reached its flexural strength. On the other hand, specimens with longer RC stub lengths of 1.5*D* and 2.0*D* failed due to tensile rupture of the GFRP tube at the end of the RC stub (Fig. 7(b)). Clearly, these two specimens achieved the full flexural strength of the CFFT.

The load-slip behavior of the specimens is shown in Fig. 6(b). This 'slip' includes the crack opening of the RC stub at the face of the footing plus any slip experienced by the tube relative to the stub on the tension side. Given the identical and very heavy steel reinforcement ratio in the stubs of all four specimens, the crack opening at failure is quite small. Specimens M-1.5D-S9 and M-2.0D-S9 with sufficiently long stubs and failing by tube rupture suggest that this crack opening at ultimate is about 1.0 mm or less at lower loads (Fig. 6(b)). As such, the measured much larger values of 'slip' in the other two specimens (M-0.5D-S9 and M-1.0D-S9) are primarily the relative slip between the tube and RC stub. Figure 6(a) demonstrates a steady rate of load increase for these two specimens until reaching their peak loads of 4.9 kN and 17.6 kN, respectively. Both specimens then experienced gradual load drop with an increased slip. Close inspection of the specimens revealed that bond failure did not occur in the adhesive layer, but a layer of the concrete cover of the stub remained adhered to the inner surface of the tube. This explains the gradual load drop as a result of the shear friction and aggregate interlock. This in turn resulted in the apparent pseudo-ductile load-deflection behavior in Fig. 6(a). Figure 6(c) shows that the longitudinal strains in the tube at stub end were lower than the 0.02 rupture strain when bond failure occurred, though specimen M-1.0D-S9 was very close to a flexural failure. In specimen M-1.0D-S9, the excessive slip (Fig. 7(a)) was followed by a secondary tensile rupture of the tube in the hoop direction on the compression side.

Specimens M-1.5D-S9 and M-2.0D-S9 both failed due to tensile rupture of the tube (Fig. 7(b)) at the RC stub ends. Longitudinal strains at this location (Fig. 6(c)) show very comparable values of 0.021 and 0.019 for specimens M-1.5D-S9 and M-2.0D-S9, respectively. Figure 6(a) shows a gradual increase in load up to the peak values of 20.5 kN and 23.5 kN for specimens M-1.5D-S9 and M-2.0D-S9, respectively, where flexural tension failure occurred. Beyond the first cracking that occurred at about 2 kN, specimen M-2.0D-S9 demonstrates a slightly higher yet noticeable stiffness, due to the longer RC stub. The small frequent load drops are due to subsequent flexural cracking in the CFFT at various locations. The very small 'slip' values measured in Fig. 6(b) are essentially a reflection of the very small crack opening at the stub-footing junction as these specimens did not suffer any bond failure.

Optimal RC Stub Length: Figure 8 shows the variation of the moments corresponding to peak loads versus the RC stub length X normalized to the CFFT diameter D (X/D). The moments are calculated at the end of the RC stubs in all specimens, a location that governs the failure mode corresponding to the CFFT, which is the maximum potential strength of the system. For specimens failing by CFFT tube rupture, the moment at stub end would always be the same regardless of stub length, whereas in specimens failing by bond, the moment at stub end will be reduced as stub length becomes shorter. Figure 8 shows a clear increase in the moment with increasing the RC stub length from 0.5D to 1.0D, up to a certain flat ceiling where flexural failure governs at 1.5D and 2D. To establish the ceiling, the average ultimate moments of specimens failing in flexure was considered. Since specimen M-1.5 D-S4 (from Phase II) also failed in flexure, it was added in Figure 8 to enhance the average flexural strength. The critical RC stub length then is the point at which the flexural tension failure and bond failure occur simultaneously. A parabolic fitting curve was used to connect points representing specimens M-

0.5D-S9, M-1.0D-S9 and the origin. The intersection of this curve with the flat plateau of the average flexural strength occurs at a critical stub length (X_{cr}) of 1.05D. It is important to note that X_{cr} depends on the geometric and mechanical properties of the CFFT system as will be studied analytically at a later section of this paper.

The Effect of Steel Reinforcement Ratio in Stub

The specimens in Phase II and specimen M-1.5D-S9 from Phase I, had three different steel reinforcement ratios in the RC stubs, but all had an equal stub length of 1.5D. This length was selected based on the findings of Phase I, to be larger than X_{cr} to avoid bond failure. Figure 9 shows a comparison of the following responses: load-deflection, load-slip, and load-longitudinal strains of the tube at the end of the RC stub.

Ductile versus Brittle Failure: Specimen M-1.5D-S2 failed due to excessive yielding of the steel reinforcement, associated with excessive deflection. The significant concrete confinement has lead to development of a plastic hinge, manifested by a large crack at the RC stub-footing junction and a very ductile load-deflection response (Fig. 9(a)). Failure mode of specimen M-1.5D-S2 is shown in Fig. 7(c), while failure of specimen M-1.5D-S9 was discussed earlier (Fig. 7(b)). Specimen M-1.5D-S4 also developed some yielding of the reinforcement and some ductility (Fig. 9(a)), however, the CFFT eventually failed by rupture of the tube at the end of the RC stub. Specimen M-1.5D-S9 was very heavily reinforced such that the load-deflection was almost linear without any ductility, until the tube fractured at the end of the stub. Figure 9(a) clearly shows the increase in stiffness as the steel reinforcement ratio increased.

Figure 9(b) shows the load-slip behaviors for the three specimens. Since the stub length was sufficient to avoid any bond failure of the tube in these specimens, the ‘slip’ in Fig. 9(b) represents mainly the crack opening at the footing-stub junction. An excessive increase in crack

opening in specimens M-1.5D-S2 and M-1.5D-S4 is associated with the onset of yielding of the steel reinforcement. It is also possible that excessive yielding of the steel bars was associated with some localized slip within the stub. However, given the significant confinement in the RC stub it is believed that bond of steel rebar was quite enhanced.

The load-strain behavior of the tube at the RC stub end is shown in Fig. 9(c). Ultimate tensile strains of 0.021 and 0.023 were reached in the tubes of specimens M-1.5D-S9 and M-1.5D-S4, respectively, at the end of stub at rupture. Specimen M-1.5D-S2 reached a maximum tensile strain of only 0.01 in the tube, at the end of the excessive deflection. This clearly indicates that this specimen was far from failing of the CFFT section. On the compression side, specimens M-1.5D-S9 and M-1.5D-S4 reached -0.012 and -0.014 at the end of the RC stub, while specimen M-1.5D-S2 reached -0.007. It is very clear that the tube provides significant confinement for concrete in compression as evident by these longitudinal strains far exceeding the typical crushing strain of -0.003 of unconfined concrete.

Optimal Reinforcement Ratio: It is clear from Fig. 9(a) that for a given GFRP tube, the amount of steel reinforcement at the connection significantly affects strength and ductility. If the design is intended to be 'ductility-controlled', a lower steel ratio associated with lower strength may be used. In this case the GFRP tube may be underutilized. On the other hand, if large ductility is not a requirement and a 'strength-control' design with moderate ductility is acceptable, increasing the steel reinforcement may be desired. In this case, failure is governed by the GFRP tube and increasing the steel ratio beyond a certain limit will not be useful. The goal of this section is to establish the maximum steel ratio that would allow the CFFT to achieve its full flexural strength.

Figure 10 shows a variation of the maximum moment reached at the footing face with the steel reinforcement ratio (ρ_s) of the RC stub for the three specimens. An additional hypothetical

point is added at (ρ_s = 0) which is essentially the cracking moment of a plain concrete stub, calculated using a modulus of rupture of $0.6\sqrt{f_c'}$. By extending a line connecting this point (ρ_s = 0) and the point representing M-1.5D-S2, until it intersects a flat plateau representing the average of M-1.5D-S4 and M-1.5D-S2, a point representing an optimal reinforcement ratio (ρ_{opt} = 3.2%) is achieved. This steel ratio allows the designer to take advantage of the full CFFT flexural capacity, while achieving some ductility. Members with any higher steel ratio will not gain any further strength, but rather will loose ductility. On the other hand, members with lower steel ratio will gain more ductility but will loose strength.

Testing under Low-Cyclic Fatigue

Specimens C-1.5D-S2 and PC-1.5D-S2 were tested under reversed cycling loading. Initially, up to yielding, loading was applied incrementally to certain fractions of the yielding load P_y. After yielding, loading was applied as increments of the deflection at yield Δ_y. Table 3 summarizes the cyclic loading regime for both specimens. Two full cycles under each load level (or ductility level) were completed. Specimen C-1.5D-S2 was tested under reversed cyclic loading without any axial loads. This represents applications governed primarily by flexure such as utility and light poles. Specimen PC-1.5D-S2 was subjected to an axial compressive load of 234 kN. This represents 15% of the pure axial strength of the CFFT member, which was established based on an ancillary axial loading test on a 700 mm long CFFT stub. However, as the deflections increased during various cycles, the resulting elongation of the prestressing strands caused some increase in the applied axial load, up to 300 kN. At this point, the specimen was already sufficiently yielded and the test was terminated for safety reasons. Testing of Specimen C-1.5D-S2 ended due to excessive deflection after the peak load was reached and started dropping. Neither specimen failed due to tensile rupture or slippage of the tube from the RC stub. Rather,

excessive yielding took place as a result of the formation of a plastic hinge near the footing. This was evident by a large crack at the stub-footing junction. The opening and closing of this crack during reversed loading cycles was clearly visible and resulted in concrete spalling near the end.

Load-Deflection Responses: Figures 11 (a) and (b) show the load-deflection hysteretic responses for the two specimens, while Fig. 11(c) shows the envelope of the load-deflection responses, compared with monotonically loaded specimen M-1.5D-S2. From these curves, it can be seen that the load-deflection response for specimens C-1.5D-S2 reached the maximum load of 12.6 kN at ductility ratio of $2\Delta_y$ and remained relatively stable up to $5\Delta_y$, then gradually dropped in subsequent cycles, as a result of the cumulative local damage. The load drop at the second cycle of each loading increment gets more pronounced at higher load levels beyond yielding. For the final full cycle of $6.5\Delta_y$, the load drop in second cycle was 39%. Figure 11(c) shows that, in comparison with the monotonic testing of specimen M-1.5D-S2, the main difference is the inability of specimen C-1.5D-S2 to maintain its peak load. The ductility achieved at the peak load was at least $8\Delta_y$ for specimen M-1.5D-S2, when the test was terminated, while it was $5\Delta_y$ for specimen C-1.5D-S2, before the load started to decline.

Based on Fig. 11(b) for specimen PC-1.5D-S2, the hysteretic response clearly reflects yielding of the steel reinforcement. However, beyond yielding the load continued rising gradually and reached 24.7 kN on the last cycle at a ductility ratio of $4\Delta_y$ when the test was terminated for safety concerns. As mentioned, additional tension forces built up in the post-tensioning steel strands. This undoubtedly caused the continued rising of the transverse load capacity of the specimen. The strength of the specimen would have stabilized if the axial load remained constant. For this specimen, the second cycle in each loading step reached a slightly lower peak load than the first cycle, as was also observed in specimen C-1.5D-S2. This is due to

some energy loss as a result of the reversed cyclic loading. However, this was rather a slight drop compared to specimen C-1.5D-S2. At the cycle of $1\Delta_y$, this drop was 3.7%, and increased slightly to 6% at the cycle of $6\Delta_y$. This is a far contrast from the 39% drop demonstrated by specimen C-1.5D-S2 at the cycle of $6.5\Delta_y$.

Effect of Axial Load: It is clear from the load-deflection hysteretic curves for the two specimens, that the presence of an axial compression load has a large effect on the load-deflection behavior of the specimens. The axial load, which ranged from 15 to 19% of the axial strength of the CFFT, had a very noticeable effect on the behavior. A 96% increase in the peak load was observed in specimen PC-1.5D-S2, relative to C-1.5D-S2 (Fig. 11). Additionally, the axial load delayed first cracking and caused the cracks to close upon unloading, which made specimen PC-1.5D-S2 stiffer. As mentioned earlier, the strength of specimen C-1.5D-S2 began to decrease at a ductility ratio of $5\Delta_y$, while the strength of specimen PC-1.5D-S2 continued to increase gradually throughout the test. It is clear that the presence of a small axial load has resulted in stabilizing the system, as evident by the smooth and more stable hysteretic curves. Clearly, both specimens demonstrated some pinching effect, which is more pronounced in specimen C-1.5D-S2 than in PC-1.5D-S2, as the axial load limits the amount of local slippage of the steel rebar.

ANALYTICAL MODELING

Figure 12 shows a free body diagram of the tube bonded to the stub of length X. Assuming that the primary mechanism of moment transfer between the tube and stub is by bond, the shear stress distribution is established as shown, with the amplitude being τ_{max}. The resultant force F of the shear stress distribution can be calculated using Eq. 1, and is balanced by an equal and opposite bearing force between the bottom edge of the tube and the footing.

$$F = D_i \int_{x=0}^{x=X} \int_{\theta=0}^{\theta=\pi} 0.5\tau_{max}(1+\cos\theta)\, d\theta\, dx = \frac{\pi}{2} D_i\, X\, \tau_{max} \quad (1)$$

The resulting moment M at end of stub can be calculated as follows:

$$M = D_i^2/2 \int_{x=0}^{x=X} \int_{\theta=0}^{\theta=\pi} 0.5\tau_{max}(1+\cos\theta)\cos\theta\, d\theta\, dx + F\, D_i/2 = \frac{3\pi}{8} D_i^{\,2}\, X\, \tau_{max} \quad (2)$$

where D_i is the inner diameter and X is the length of stub. From Eq. 2, the required stub length X for any applied moment M can be found as follows:

$$X = \frac{8M}{3\pi\tau_{max} D_i^2} \quad (3)$$

As discussed earlier, it was observed in the experiments that shear failure occurs within a layer of the concrete cover and not at the adhesive bond layer. Therefore, the shear strength τ_{max} is calculated based on the model by Vecchio and Collins (1986) as the following:

$\tau_{max} = 0.18\tau_o + 1.64\sigma - 0.82\sigma^2/\tau_o$, where:

$$\tau_o = \frac{\sqrt{f_c'}}{0.31 + 24w/(a+16)} \quad (4)$$

f_c' is the concrete compressive strength, w is the crack width and in this case is assumed zero, since the tube fits tightly, a is the maximum aggregate size. σ is the normal stress acting on the shear failure surface, which is insignificant in this case as confinement in a CFFT system primarily subjected to flexure was shown to be very weak (Fam et al, 2003). As such, Eq. 4 can be reduced to the following expression:

$$\tau_{max} = 0.58\sqrt{f_c'} \quad (5)$$

For CFFTs failing in flexure by rupture of the tube, Fam and Son (2008) proposed the following equation for the ultimate moment M_u:

$$M_u = 0.0045 D_o^{\,3} f_c' \left(100 \frac{4t}{D_o} \frac{f_{tu}}{f_c'} \right)^{0.815} \quad (6)$$

where f_{tu} is the ultimate tensile strength of the tube and D_o is the outer diameter.

By setting the moment at bond failure in Eq. 3 at the end of stub, equals the moment at flexural failure from Eq. 6, and using an average diameter D in both equations, the critical stub length X_{cr} required to achieve flexural and bond failure simultaneously can be established:

$$\left(\frac{X}{D} \right)_{cr} = 0.5 \frac{f_c'}{\tau_{\max}} \left(\frac{t}{D} \frac{f_{tu}}{f_c'} \right)^{0.815} \quad (7)$$

Equations 3 and 6 were used to predict the variation of moment with stub length ratio (X/D), as shown in Fig. 8, which showed reasonable agreement with test results. Figure 8 and Eq. 7 show that the predicted critical $(X/D)_{cr}$ ratio is 1.24, while experimental trends suggest 1.05.

A parametric study was carried out to investigate the effect of key geometric and mechanical parameters on $(X/D)_{cr}$, namely (D/t) ranging from 30 to 150, f_{tu} ranging from 100 to 1000 MPa, and f_c' ranging from 20 to 80 MPa. Figure 13 summarizes the results of this study. It can be concluded that $(X/D)_{cr}$ reduces as (D/t) increases. The rate of this reduction increase as f_{tu} and f_c' increase. Also, for a given (D/t), $(X/D)_{cr}$ reduces as f_{tu} and f_c' reduce.

SUMMARY AND CONCLUSIONS

Eight medium-scale cantilever-bending CFFT-footing specimens were constructed and tested with an emphasis on a new moment connection. Prefabricated GFRP tubes were adhesively bonded to short RC stubs protruding from the footing and tightly matching the tube inner diameter. The effects of RC stub length, steel reinforcement ratio in the stub, and reversed cyclic bending have been studied. Also, a simple design model has been developed to predict the

moment at bond or flexural failure, as well as the minimum stub length required to achieve the full flexural strength of the CFFT. The following conclusions are drawn:

1. For the CFFT tested herein, the critical stub length-to-diameter $(X/D)_{cr}$ ratio was 1.05. This represents the minimum length necessary for the CFFT to fail in flexural just beyond the stub, hence allowing the system to achieve its full potential. A smaller (X/D) leads to bond failure at lower capacity, while a larger (X/D) does not provide any further gain in strength. However, $(X/D)_{cr}$ depends on the tube and concrete geometric and mechanical properties.
2. $(X/D)_{cr}$ reduces as the tube diameter-to-thickness ratio increases, and as the tube longitudinal tensile strength and concrete compressive strength reduce. However, $(X/D)_{cr}$ is much more sensitive to the tube strength than to the concrete strength.
3. For the CFFT tested herein, an optimal longitudinal steel reinforcement ratio ρ_s of 3.2% was required in the stub in order for the CFFT to reach its full flexural strength just beyond the stub. Higher ρ_s did not provide any gain in strength, but rather loss of ductility. The optimal ρ_s will vary as the CFFT mechanical and geometric properties change.
4. The specimen with ρ_s in the stub equals to 2%, less than the optimal ρ_s, resulted in more ductility but lower strength due to underutilization of the CFFT member. A plastic hinge was formed at the junction with footing, facilitated by concrete confinement on compression side.
5. The peak load under reversed low-cycle fatigue bending of the specimen without axial compression loads was attained at ductility ratio of 2 and began degrading beyond ductility ratio of 5. In the final cycle, at a ductility ratio of 6.5, the load had dropped by about 40%. .
6. The presence of a small axial load of 15-20% of the CFFT axial compressive strength significantly enhances performance under reversed cyclic bending. It resulted in almost doubling the capacity, and produced a much more stable hysteretic behavior.

7. The proposed connection and construction method eliminates the need for any shoring of the tube during curing of adhesive and indeed during concrete filling and curing. However, potential corrosion of the steel reinforcement in the stub remains a threat. Galvanized or stainless steel may be used for the stub reinforcement.

ACKNOWLEDGEMENTS

The authors wish to acknowledge NSERC, the Canada Research Chairs program, The Early Researcher's Award Program of the Ontario Government, and Queen's University for the Chancellor's Research Award. The authors are also grateful to Paul Thrasher and David Tryon from Queen's University.

REFERENCES

1. Mirmiran, A., and Shahawy, M. (1997). "Behavior of concrete columns confined by fiber composites." *J. Struct. Eng.*, 123(5), 583–590.
2. Fam, A. Z., and Rizkalla, S. H. (2002). "Flexural behavior of concrete-filled fiber-reinforced polymer circular tubes." *J. Compos. Constr.*, 6(2), 123–132.
3. Zhu, Z., Mirmiran, A., and Shahawy, M. (2004). "Stay-in-place fiber reinforced polymer forms for precast modular bridge pier system." *J. Compos. Constr.*, 8(6), 560–568.
4. Zhu, Z., Ahmad, I., and Mirmiran, A. (2006). "Seismic performance of concrete-filled FRP tube columns for bridge substructure." *J Bridge Eng.*, 11(3), 359–370.
5. Qasrawi, Y., and Fam, A. (2008). "Flexural load tests on new spun-cast concrete-filled fiber-reinforced polymer tubular poles." *ACI Struct. J.*, 105(6), 750–759.

6. Fam, A. (2008). “Development of a novel pole using spun-cast concrete into FRP tubes.” *PCI J.*, 53(3), 100–113.
7. Nelson, M., Lai, Y. C., and Fam, A. (2008). “Moment connection of concrete-filled fiber reinforced polymer tubes by direct embedment into footings.” *Advances Struct. Eng.*, 11(5), 537–547.
8. Sadeghian, P., and Fam, A. (2010). “Bond-slip analytical formulation towards optimal embedment of concrete-filled circular FRP tubes into concrete footings.” *J. Eng. Mech.*, 136(4), 524–533.
9. Sadeghian, P., and Fam, A. (2010). “Closed-form model and parametric study on connection of concrete-filled FRP tubes into concrete footings by direct embedment.” *J. Eng. Mech.*, submitted.
10. Lai, Y. C. (2010). “Moment connections of concrete-filled fibre reinforced polymer tubes to reinforced concrete footings.” MSc thesis, Queen’s Univ., Kingston, Ontario, Canada.
11. Fam, A., and Son, J.K. (2008). “Finite element modeling of hollow and concrete-filled fiber composite tubes in flexure: Optimization of partial filling and a design method for poles,” Engineering Structures, 30(10), 2667–2676

Table 1. Test matrix

Phase	Specimen ID[1]	RC stub length (mm)	RC stub steel reinforcement	RC stub steel reinforcement ratio (%)	Axial load (kN)	Lateral load type
I	M-0.5D-S9	85 (0.5D)	6-20M[2]	8.73 (~9)	0	Monotonic
	M-1.0D-S9	169 (1.0D)	6-20M	8.73 (~9)	0	Monotonic
	M-1.5D-S9	253 (1.5D)	6-20M	8.73 (~9)	0	Monotonic
	M-2.0D-S9	338 (2.0D)	6-20M	8.73 (~9)	0	Monotonic
II	M-1.5D-S2	253 (1.5D)	4-10M	1.94 (~2)	0	Monotonic
	M-1.5D-S4	253 (1.5D)	4-15M	3.88 (~4)	0	Monotonic
III	C-1.5D-S2	253 (1.5D)	4-10M	1.94 (~2)	0	Cyclic
	PC-1.5D-S2	253 (1.5D)	4-10M	1.94 (~2)	234-300	Cyclic

[1] Specimen IDs: M=monotonic loading, C=cyclic loading, P=post-tensioned, S=steel reinforcement ratio of RC stub, D=tube outer diameter (169 mm).
[2] 10M=100 mm^2, 15M=200 mm^2, and 20M=300 mm^2

Table 2. Summary of test results

Specimen ID	Peak Load (kN)	Peak moment at sec. ***a*** (kN-m)	Peak moment at sec. ***b*** (kN-m)	End Deflection at peak load (mm)	Slip at peak load (mm)	Tube longitudinal strain at peak load at sec. ***b*** (mm/mm)		Failure mode (location)
						Top	Bottom	
M-0.5D-S9	4.91	6.38	5.97	35.5	2.4	0.002	-0.004	**B (*a*-*b*)**
M-1.0D-S9	17.61	22.89	19.92	109.7	4.5	0.016	-0.009	**B (*a*-*b*)+H(*a*)**
M-1.5D-S9	20.48	26.62	21.43	108.0	1.4	0.021	-0.012	**F (*b*)**
M-2.0D-S9	23.51	30.56	22.62	116.0	1.1	0.019	-0.011	**F (*b*)**
M-1.5D-S2	12.52	16.28	13.10	271.0	-	0.010	-0.007	**Y (*a*)**
M-1.5D-S4	18.91	24.58	19.79	238.0	-	0.023	-0.014	**Y (*a*)+F (*b*)**
C-1.5D-S2	12.55	16.32	13.14	150.2	-	0.0106	-0.0065	**Y (*a*)**
PC-1.5D-S2	24.66	32.06	25.81	151.0	-	0.0144	-0.0066	**Y (*a*)**

a: section at column-footing interface
b: section at the end of RC stub
B: bond failure
F: flexural failure of CFFT
H: hoop failure of tube
Y: yielding of RC stub

Table 3. Summary of cyclic loading regime for specimens in Phase III

	Specimen C-1.5D-S2			Specimen PC-1.5D-S2		
Cycle	Load control	Stroke control	Load rate (mm/min)	Load control	Stroke control	Load rate (mm/min)
1	2.19 kN ($0.3P_y$)	-	1.5	4.10 kN ($0.3P_y$)	-	1.5
2	3.65 kN ($0.5P_y$)	-	1.5	7.20 kN ($0.5P_y$)	-	1.5
3	7.30 kN ($0.7P_y$)	-	5.0	14.50 kN ($1.0P_y$)	20 mm ($1.0\Delta_y$)	5.0
4	10.30 kN ($1.0P_y$)	30 mm ($1.0\Delta_y$)	5.0	-	40 mm ($2.0\Delta_y$)	5.0
5	-	60 mm ($2.0\Delta_y$)	5.0	-	70 mm ($3.5\Delta_y$)	15.0
6	-	90 mm ($3.0\Delta_y$)	15.0	-	100 mm ($5.0\Delta_y$)	15.0
7	-	120 mm ($4.0\Delta_y$)	15.0	-	150 mm ($7.5\Delta_y$)	30.0
8	-	150 mm ($5.0\Delta_y$)	30.0	-	-	-
9	-	200 mm ($6.5\Delta_y$)	30.0	-	-	-

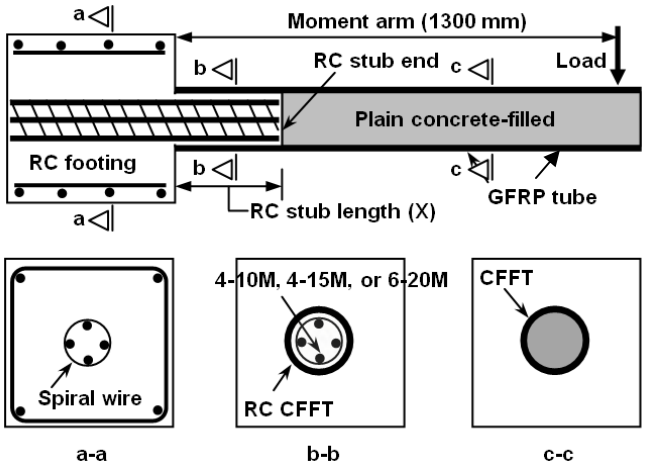

Fig. 1. Schematic of a typical test specimen

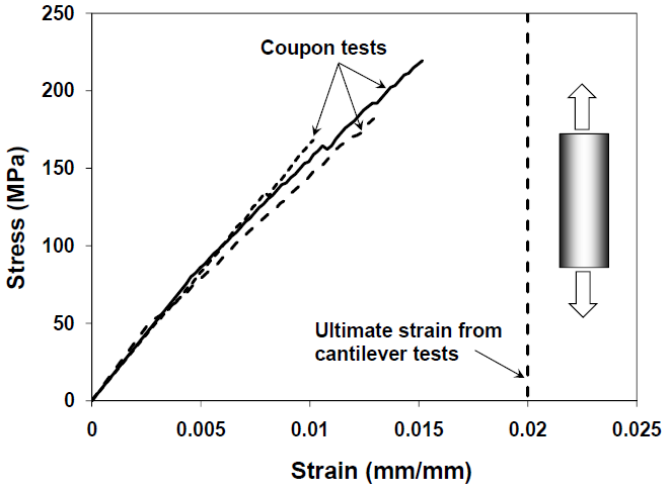

Fig. 2. Stress-strain curves of GFRP tube in longitudinal direction

Fig. 3. Preparation of RC footings and stubs

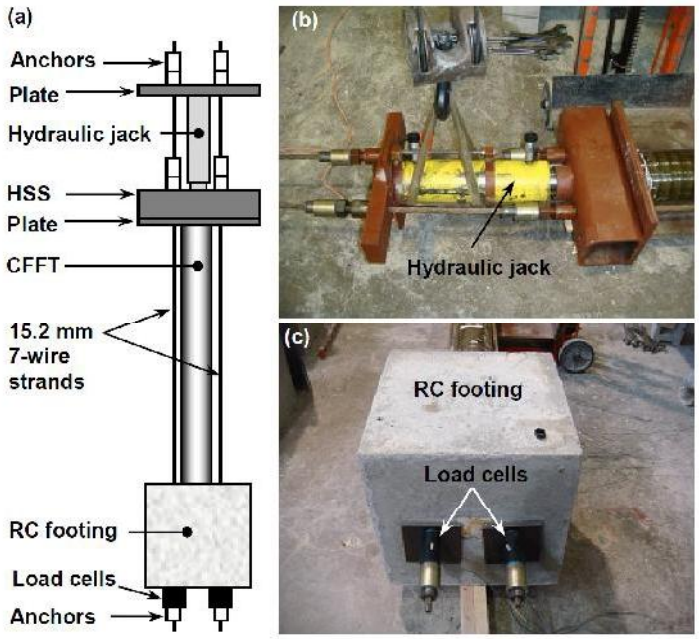

Fig. 4. Post-tensioning of specimen PC-1.5D-S2: (a) setup, (b) jacking at top end, and (c) anchors and load cells at dead end

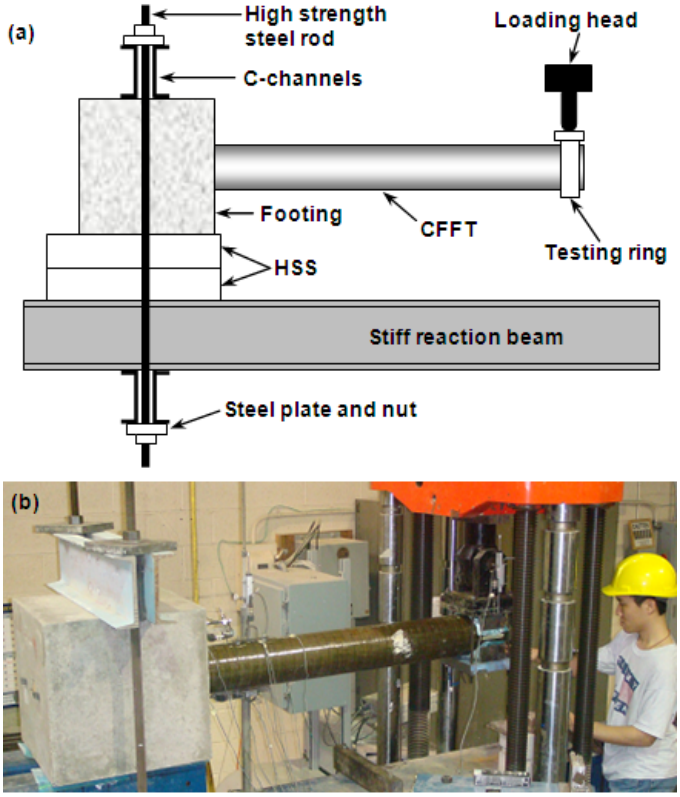

Fig. 5. Test setup

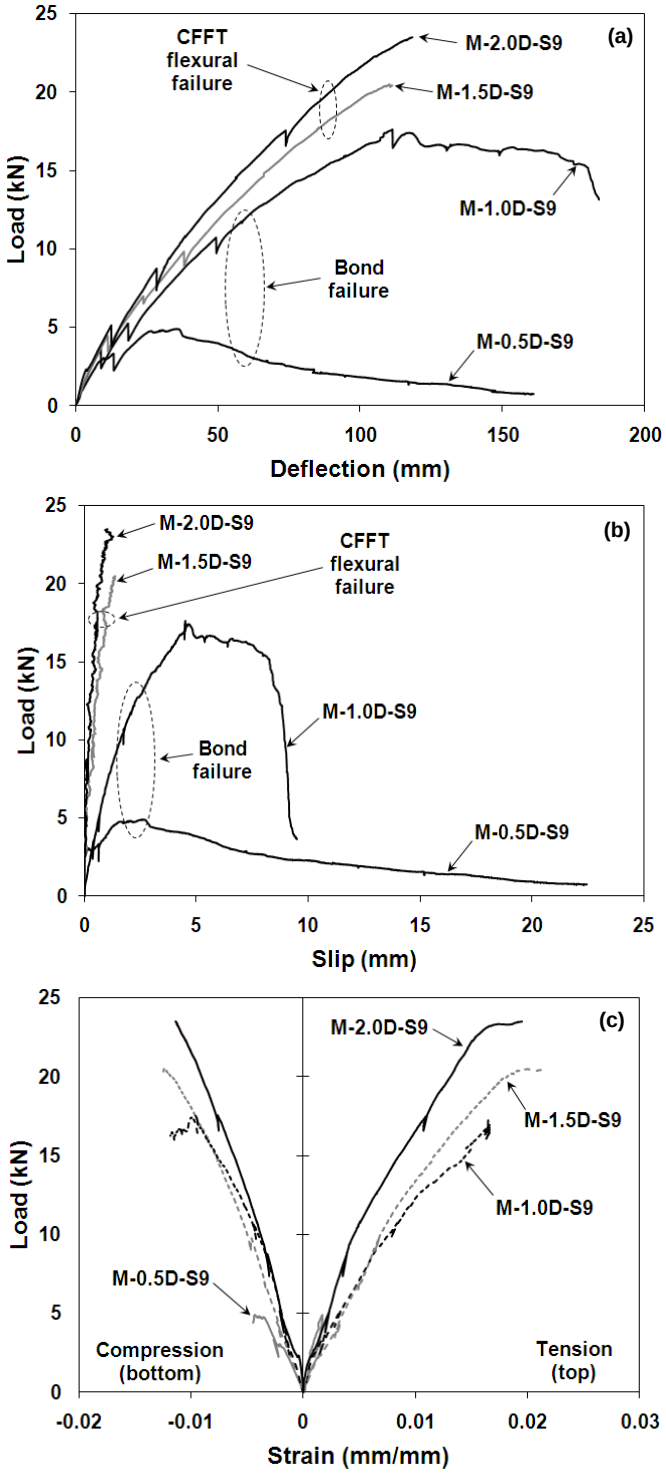

Fig. 6. Responses of specimens with different RC stub lengths (Phase I): (a) load-deflection, (b) load-slip and (c) load-longitudinal strain at stub end

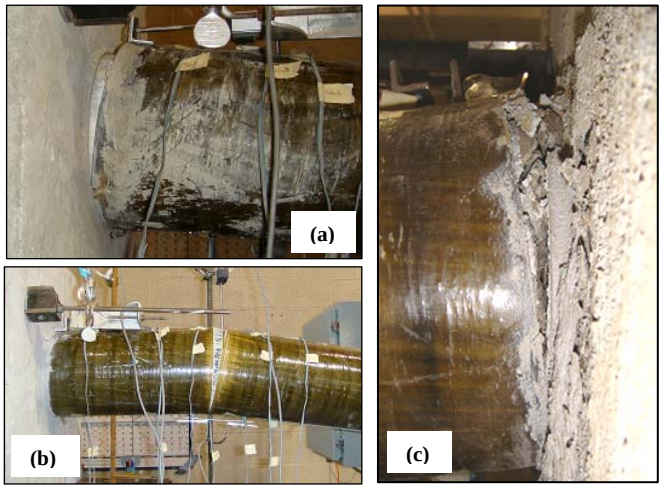

Fig. 7. Sample failure modes: (a) bond failure (slip) of M-1.0D-S9, (b) CFFT flexural tension failure of M-2.0D-S9, and (c) excessive steel yielding in M-1.5D-S2

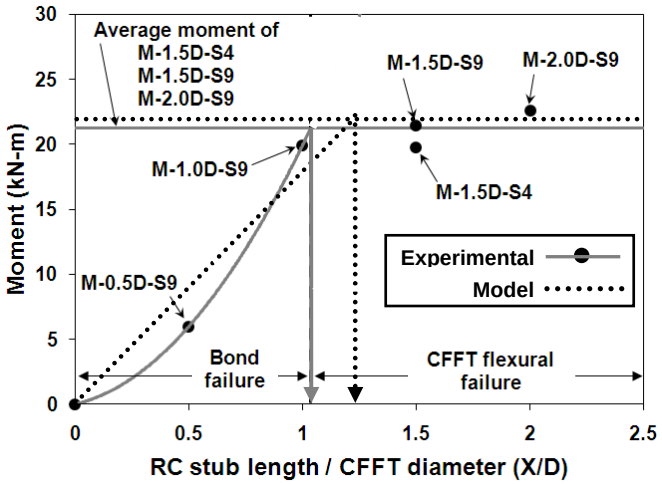

Fig. 8. Variation of peak moment at stub end with stub length

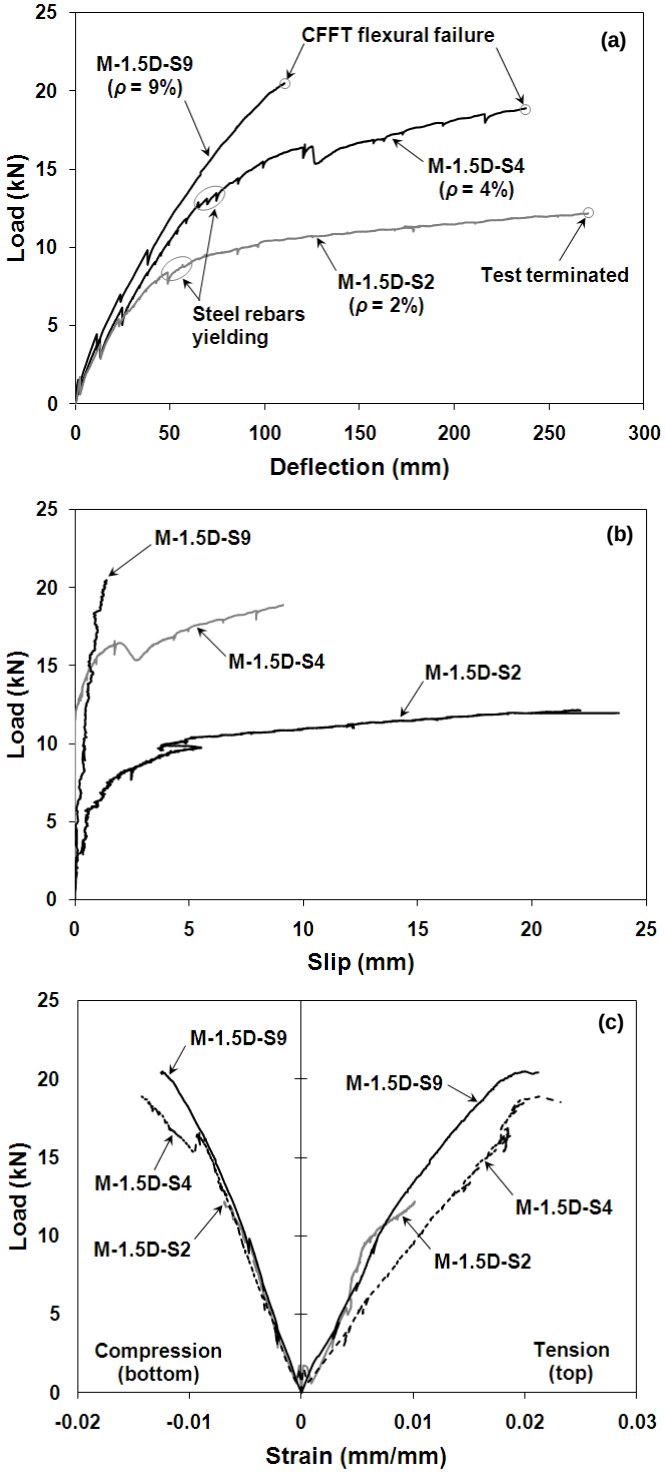

Fig. 9. Responses of specimens with different steel reinforcement ratios in the stubs: (a) load-deflection, (b) load-slip, and (c) load-longitudinal strain responses at stub end

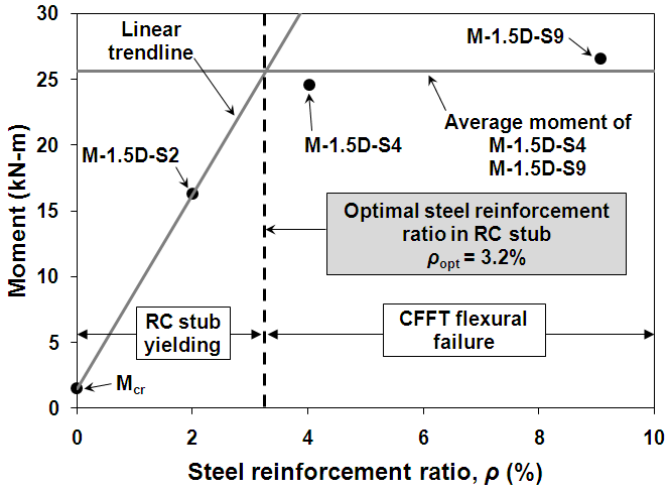

Fig. 10. Variation of peak moment at footing with steel reinforcement ratio in stub

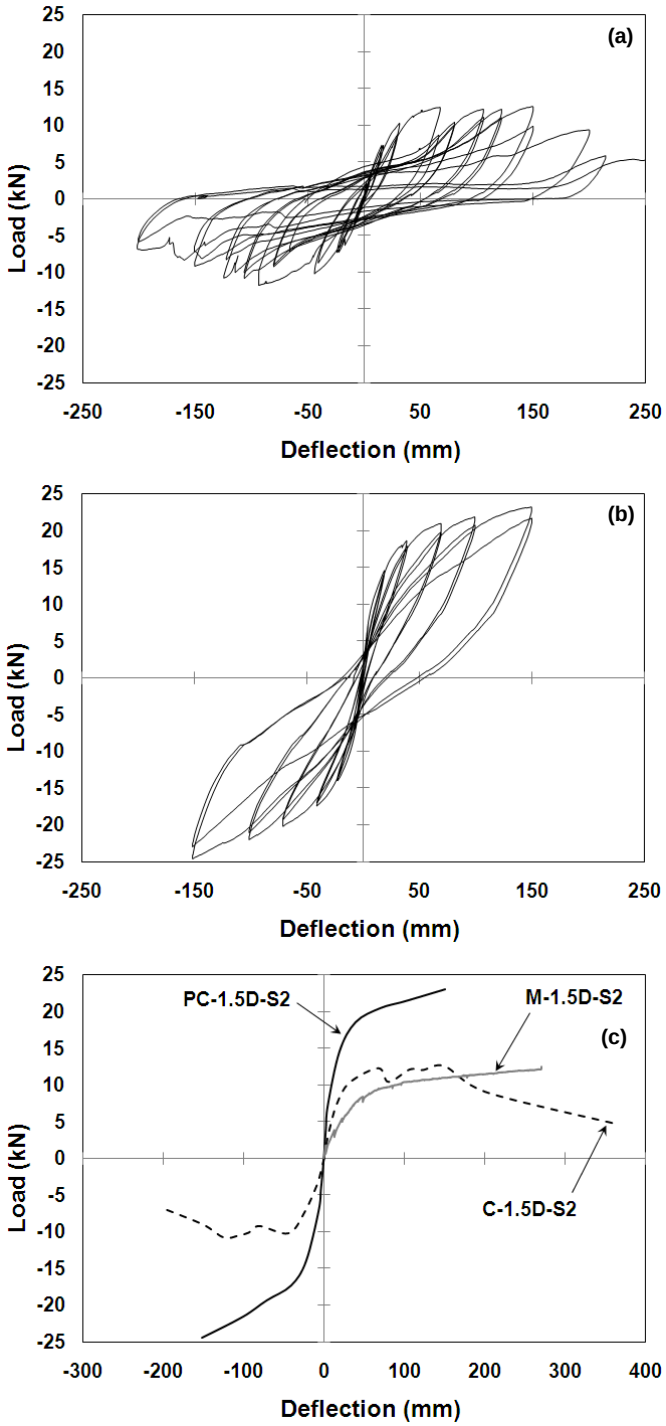

Fig. 11. Load-deflection hysteretic responses: (a) specimen C-1.5D-S2, (b) specimen PC-1.5D-S2, and (c) envelopes comparison

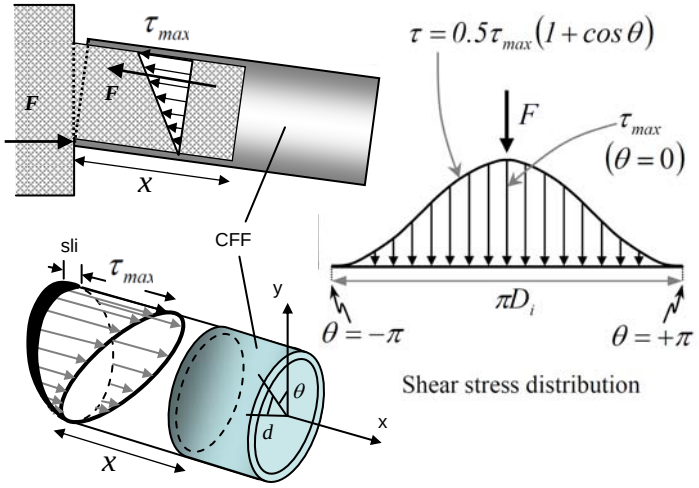

Fig. 12. Free body diagram of the analytical model

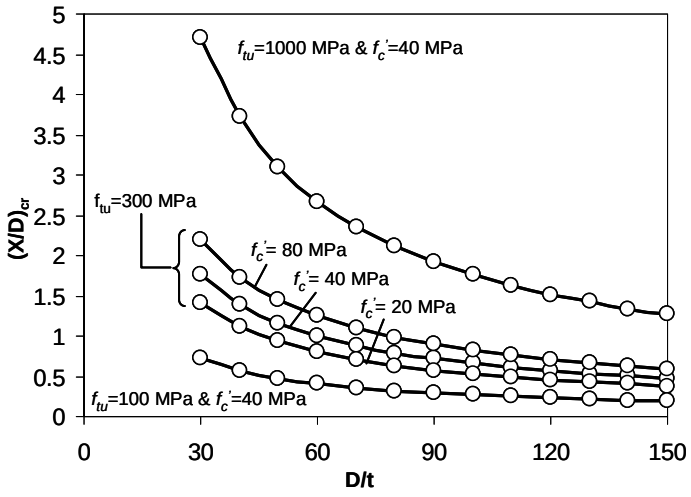

Fig. 13. Effect of various parameters on critical stub length